Chemically Modified Hydrogel-Filled Nanopores: a Tunable Platform for Single-Molecule Sensing

Dana Al Sulaiman[1], Paolo Cadinu[2], Aleksandar P. Ivanov[*2], Joshua B. Edel*[*2] and Sylvain Ladame*[*1]*

[1]Department of Bioengineering, Imperial College London, South Kensington Campus, London, SW72AZ, UK.
[2]Department of Chemistry, Imperial College London, South Kensington Campus, London, SW72AZ, UK.

[*] Corresponding authors: alex.ivanov@imperial.ac.uk (+44 2075943156), joshua.edel@imperial.ac.uk (+44 2075940754), s.ladame@imperial.ac.uk (+44 207594 5308)

KEYWORDS: single-molecule sensing, nanopore, hydrogel, DNA profiling

ABSTRACT**:**

Label-free, single-molecule sensing nanotechnologies represent ideal candidates for biomedical applications that rely on the detection of low copy number of biomolecules in small volumes of potentially complex biofluids. Among them, solid-state nanopores can be engineered that detect single molecules of charged analytes when they are electrically driven through the nanometer-sized aperture. Successfully applied to nucleic acid sensing, a fast transport in the range of 10-100 nucleotides per nanosecond often precludes the use of standard nanopores for the detection of the smallest fragments. Herein, next generation hydrogel-filled nanopores (HFN) are reported that combine quartz nanopipettes with biocompatible chemical poly(vinyl) alcohol hydrogels engineered in-house. Hydrogels were modified physically or chemically to finely tune, in a predictable manner, the transport of specific molecules. Controlling the hydrogel mesh size and chemical composition allowed us to slow-down DNA transport by four

orders of magnitude and to detect fragments as small as 100bp with nanopores larger than 20 nm, at ionic strength comparable to physiological conditions. Considering the emergence of cell-free nucleic acids as blood biomarkers for cancer diagnostics or prenatal testing, successful sensing and size profiling of DNA fragments ranging from 100bp to >1kbp long under physiological conditions demonstrates the potential of HFNs as a new generation of powerful, easily tunable, molecular diagnostics tools.

When compared to bulk measurement techniques, single molecule sensing offers the unique advantage to quantitatively detect rare species which would otherwise be lost in the noise and can, therefore, provide information on sample heterogeneity.[1] Such capability is particularly relevant to biological applications that rely on detection of minute concentrations of analytes in small volumes or even in complex biofluids. For instance, cell-free nucleic acids (cfNAs) in blood have recently emerged as non-invasive diagnostic and prognostic biomarkers for a broad range of pathologies, including cancer, but are extremely challenging to detect due to their low abundance and broad size distribution (from ~100 to 1000 nucleotides in length).[2-7]

Among the single-molecule technologies available to date, nanopore sensing has been gaining in prominence predominately due to its label-free nature and simplicity of operation. The technology measures changes in current as analytes are transported (translocated) across a nanometer-sized aperture. In recent years, nanopores were successfully applied to DNA or protein discrimination, biomolecular structure analysis, and trace analyte detection.[8]

Despite holding great promise for nucleic acid (NA) sensing, (i) it is difficult to detect cfNAs from clinical samples of complex biofluids such as blood without prior purification steps, (ii) NA fragments translocate through nanopores very quickly (up to 10-100 nt/ns)[9] making it challenging to detect short fragments, and (iii) although physically or chemically modifying nanopores can improve sensitivity and selectivity, these techniques are currently cumbersome and perhaps, most importantly, will not necessarily regulate transport of the target molecule.

For example, physical modification of the nanopore can improve sensitivity but relies on multiple fabrication steps.[10-15] Similarly, the introduction of chemical modifications to the nanopore such as charges,[13, 16] polymers[17-19] or bioreceptor[20-23] molecules, can enhance specificity and improve detection limits, but it necessitates complex functionalization protocols, frequently with low yields.[24] There is, therefore, a growing demand for the development of robust nanopores whose dimensions and chemical properties can be easily tuned to facilitate the detection of specific molecules, including short NA fragments.

Herein, we demonstrate that such tuning can be achieved by designing custom nanopore sensors using engineered hydrogel-filled nanopores (HFN). Hydrogels are traditionally used for biomedical applications including drug delivery,[25, 26] tissue engineering,[27-29] but also in biosensors, acting as matrices to encapsulate receptor probes (e.g., enzymes,[30-34] nucleic acids,[35] and even protein nanopores[36]) and enhance detection sensitivity.[37-39] Compared to other synthetic materials, hydrogels are biocompatible, antifouling (resistive to protein adsorption), and stable under physiological conditions.[40-42] More importantly, these three-dimensional networks of polymer chains are easily modified to generate hydrogels with tunable physical (i.e., mesh size or porosity) and physicochemical (i.e., charge and hydrophobicity) properties. Although a small number of biosensors combining hydrogels and physical nanopores have been reported,[43-45] they all make use of charge-free, non-chemically decorated hydrogels with mesh sizes (up to 450nm) significantly larger than the nanopore's diameter (as small as 5nm). Moreover, in two of these cases,[43, 44] the hydrogel was introduced on the cis side of the nanopore, meaning that DNA translocation occurred from the gel phase to the liquid phase. Although translocation speed was reduced by up to 100-fold slower compared to the bare nanopore, the non-uniform motion of DNA within the hydrogel prior to translocation resulted in a broad heterogeneity of translocation events for a single size population of DNA. It is also noteworthy that these studies were all carried out under non-physiological conditions of high salt concentration (1-1.6M KCl).

Herein, we report on a new and simple method for incorporation of hydrogels in nanopores. We combined quartz nanopipettes with the soft nature of in-house engineered UV-crosslinkable and chemically decorated hydrogels to produce a novel biosensing platform offering (i) tunable pore size and thus size selectivity, (ii) tunable chemistry and thus chemical/ionic selectivity, and (iii) improved sensitivity allowing for the size profiling of short DNA fragments (down to 100bp in length).

Poly(vinyl) alcohol (PVA) was used as the polymeric scaffold due to its high hydrophilicity, low toxicity, biocompatibility and ease of chemical functionalization. The PVA hydrogels were engineered via photoinitiated crosslinking polymerization of methacrylate moieties introduced by controlled modification of the PVA-hydroxyl groups with 2-isocyanatoethyl methacrylate (2-ICEMA) (SI Figure S1).[46] A chemically-crosslinked hydrogel offers the advantage of higher homogeneity and greater thermodynamic and mechanical stability compared to physically-crosslinked hydrogels. A small library of PVA hydrogels with tunable physical properties, including mesh sizes ranging from approximately 10 to 30 nm, were generated by varying the concentration and the level of methacrylation of the PVA fibers (Figure 1). Hydrogels with specific chemical properties were also engineered through PVA acetalization[47] to introduce either cationic (ammonium), anionic (carboxylate) or hydrophobic (phenyl) functionalities (SI Figure S1). These chemical moieties represent potential anchoring sites for receptors/probes, but they can also confer nanopores with gating properties to selectively tune the transport of ions or biomolecules. All hydrogels were purified by dialysis (MWCO 12kDa) and stored as solids after lyophilization. ^{1}H NMR was used to chemically characterize each hydrogel and assess the degrees of methacrylation and acetalization as outlined in Table 1 (SI Figure S2).

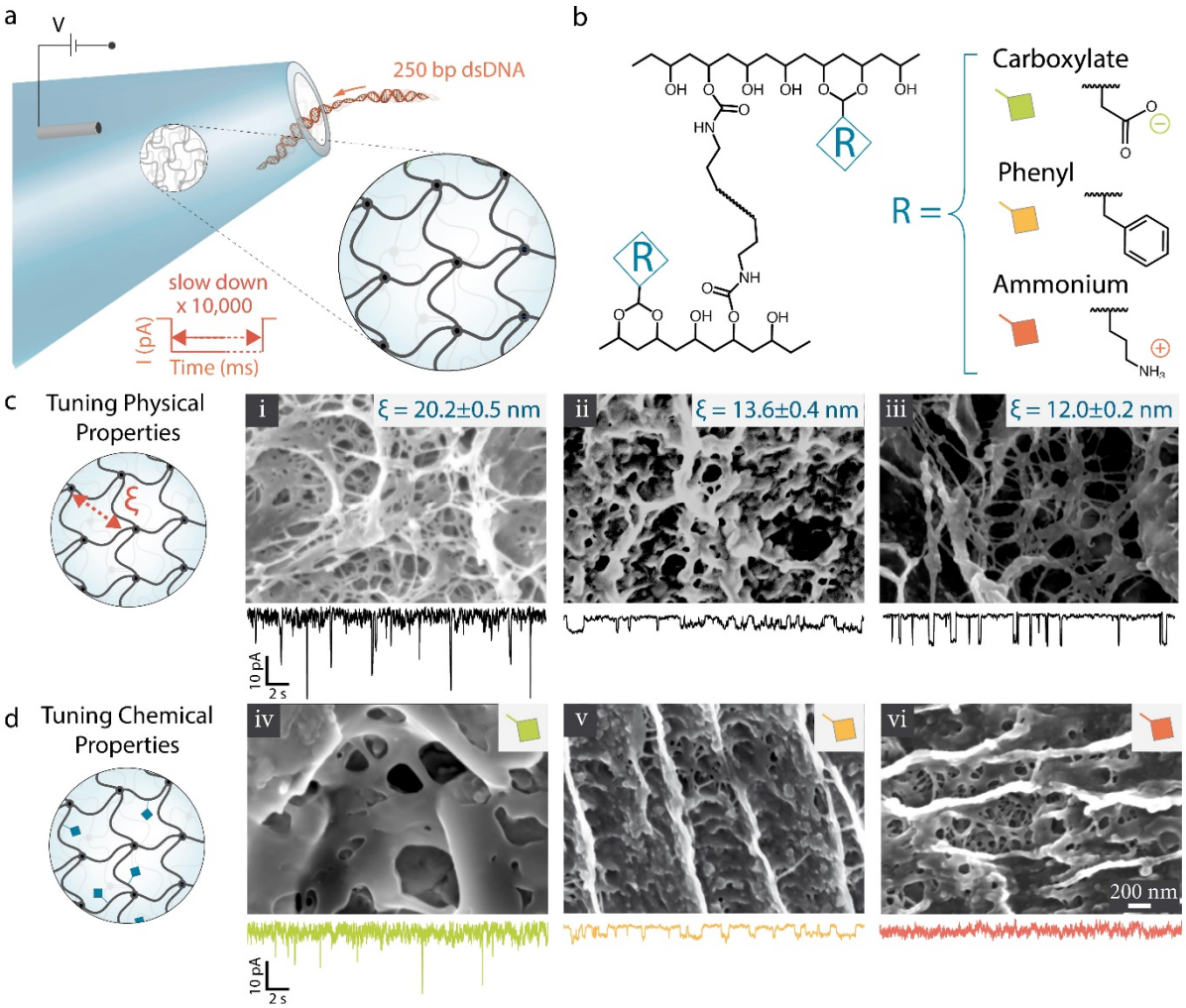

Figure 1. HFN platform design and experimental setup. (a) Schematic representation of the HFN sensor showing a crosslinked nanoporous mesh at the tip of the nanopipette and the translocation (out to in) of 250bp dsDNA. (b) Simplified chemical structure of the photo-crosslinked PVA-based hydrogels, where R represents one of the three functional groups on the chemically-modified hydrogels: anionic carboxylate functional group on PVA-CO_2^-(green), hydrophobic phenyl functional group on PVA-Phe (orange), and cationic ammonium functional group on PVA-NH_3^+(red). (c) Schematic of tuning the hydrogel physical properties (e.g. by decreasing mesh size from i to ii or iii), along with SEM micrographs (ZEISS Sigma, 5keV, 10 nm chromium coating) and current-time traces (500 mV bias) of 250bp DNA translocations within (i) unmodified PVA-OH, (ii) the higher weight percentage PVA-OH at 15 wt%, and (iii) the high methacrylate PVA-OH at 5 mol% methacrylation. (d) Schematic of tuning the hydrogel chemical properties, along with SEM micrographs and current-time traces of 250bp DNA translocations within (iv) the anionic PVA-CO_2^-, (v) the hydrophobic PVA-Phe, and (vi) the cationic PVA-NH_3^+. For visualization purposes, all traces were resampled at 20 ms (except traces iv and vi at 5 ms). Resampling rate was chosen to optimize SNR while ensuring no loss of information (SI Figure S3).

The surface structure and morphologies of all hydrogels were characterized by Scanning Electron Microscopy (SEM, Figure 1 and SI Figure S4). It is noteworthy that the hydrogel structures observed by SEM under low pressure structurally vary from the swollen, hydrated

mesh structures in solution. Thus, a more accurate investigation of the network structure and physical properties of each hydrogel was conducted via swelling and mass loss studies (SI Note S5).[26, 48-50] The network crosslinking densities and mesh sizes of all hydrogels are summarized in Table 1. Both were affected by fiber concentration (weight percentage) before polymerization, by the degree of methacrylation, and by the nature of the chemical functionality introduced on the fiber.

Hydrogel Type	PVA-OH			PVA-Phe	PVA-CO_2^-	PVA-NH_3^+
Fiber Concentration[a)]	10	15	10	15	15	15
Degree of Methacrylation[b)]	1.4	1.4	5.0	1.4	1.4	1.4
Functional groups per chain	none	none	none	4-5	1	7
Mesh Size[c)]	20.2±0.5	13.6±0.4	12.0±0.2	11.5±0.5	16.8±0.1	28.7±0.7
Crosslinking density[d)]	2.25±0.05	3.53±0.15	4.46±0.14	4.53±0.29	2.69±0.18	1.64±0.05

[a)] weight percentage (wt%); [b)] molar percentage (mol%) [c)] (nm) ± S.D. [d)] ($\bullet 10^4$ mol L^{-1}) ± S.D.

Table 1. Chemical and physical characterization of the six PVA engineered hydrogels.

Both charged hydrogels (cationic PVA-NH_3^+ and anionic PVA-CO_2^-) had mesh sizes larger than that of the bare PVA-OH formulated with the same fiber concentration and the same degree of methacrylation. This was attributed to the electrostatic repulsive forces between the charged moieties and larger hydration spheres, as previously reported with charged PVA hydrogels.[51] The effect was more pronounced with PVA-NH_3^+ than with PVA-CO_2^- (2.1 versus 1.2-fold mesh size increase) due to the 7-fold lower density of charged groups in the anionic hydrogel

compared to its cationic analog. The opposite trend was recorded for the hydrophobic PVA-Phe hydrogel with mesh sizes 1.2 times smaller than that of the bare PVA-OH. This can be attributed to the alignment and stacking of the hydrophobic aromatic groups on the otherwise hydrophilic chains acting as additional non-covalent crosslinking sites as indicated by the directional morphology observed by SEM, Figure 1d.

Using such hydrogels with tunable chemical and physical properties is therefore ideally suited to control the nanoscale transport of ions and charged biological molecules such as dsDNA. To this end, we filled the inside of quartz nanopipettes with the engineered hydrogels and studied molecular transport through the HFN. Quartz nanopipettes were fabricated using laser-assisted pipette pulling of single-barreled quartz capillaries (I.D., 0.5 mm; O.D., 1 mm; length, 7.5 cm; World Precision Instruments) using a laser pipette puller (P-2000, Sutter Instruments).[52, 53] The pulling produced a sharp tip terminating with a pore of 22 nm diameter[54] (SEM, SI Figure S6), which is (up to 2-fold) larger than the mesh size of the hydrogels (10-30 nm). Pipettes were then filled with a solution of PVA methacrylate prepared in 100 mM KCl, 10 mM Tris-EDTA (pH 8.0) solution containing 0.1 wt% of Irgacure 2959, and UV-crosslinking was performed in a BLX-315 UV crosslinker (1J Energy, 315 nm, Consort). An Ag/AgCl electrode (patch/working electrode) was then inserted inside the pipette. For all translocation experiments, the HFNs were immersed into a 100 mM KCl, 10 mM Tris-EDTA (pH 8.0) solution bath containing an Ag/AgCl ground electrode. Electrolyte ionic strength and pH chosen for nanopore sensing were near-physiological. Unless indicated otherwise, DNA translocation experiments were performed by applying a positive potential at the patch electrode, thus inducing the translocation of dsDNA from the outside to the inside of the nanopipette (i.e., from solution to hydrogel). Current vs. time traces were acquired at a 100 kHz sampling rate with a 5 kHz low-pass Bessel filter. Representative translocation data consisted of at least 130 events recorded per pipette, for at least three different pipettes under the same experimental conditions.

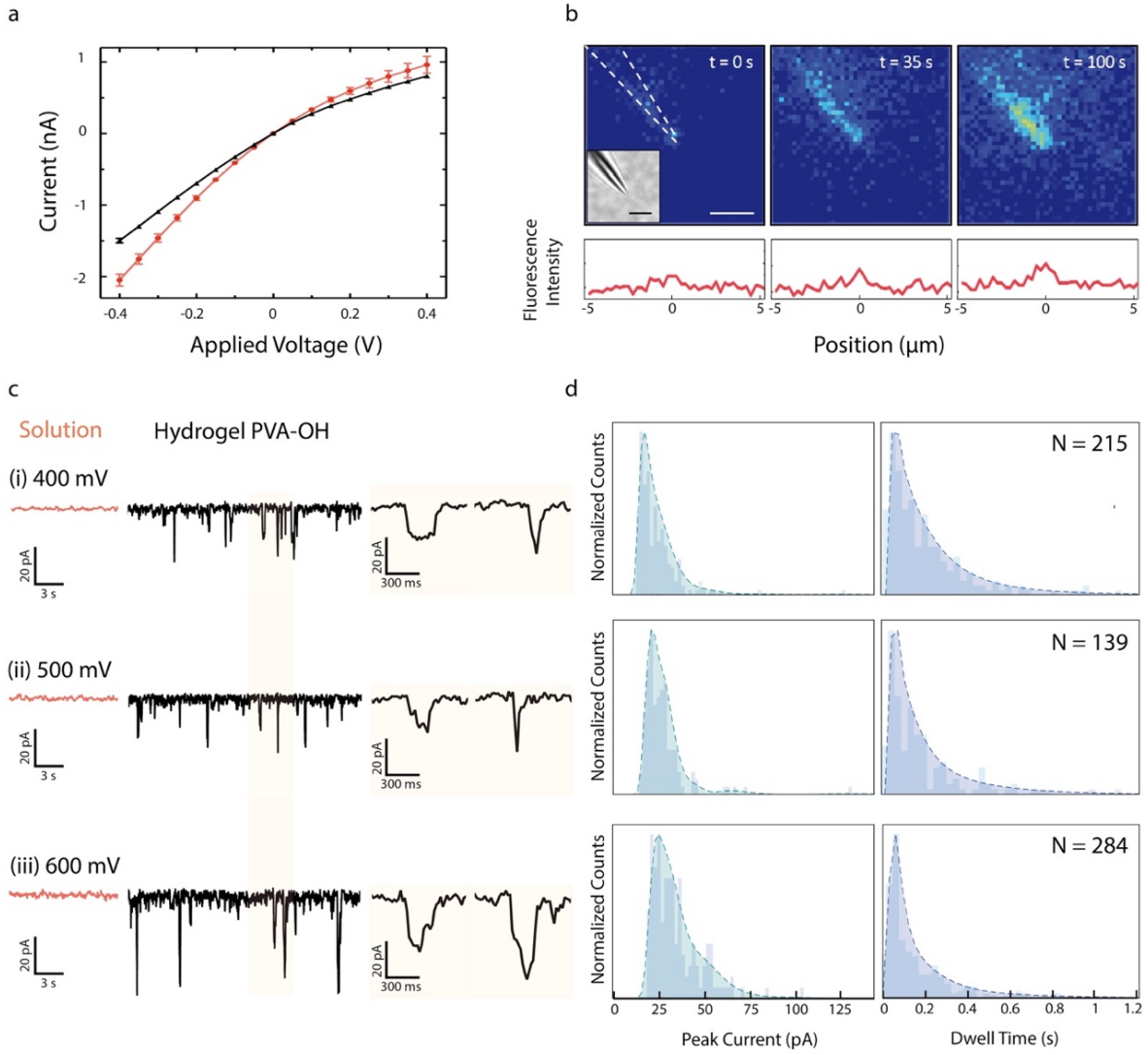

Figure 2. Electrical and optical detection of 250bp dsDNA (600 pM). (a) Average IV plots with standard error of mean bars for PVA-OH HFN (black) and standard nanopipette configuration (red), both at 100 mM KCl (SI Figure S7). Negative rectification was observed in both configurations owing to the conical geometry and the negatively charged pore walls inducing chloride anion selectivity. (b) Fluorescence images recorded with an emCCD camera (25 ms exposure time) showing that upon the application of a 1V bias after t=0s, fluorescence intensity at the HFN tip increases over time owing to DNA translocation and accumulation within the HFN. Inset on the first image shows a bright field image of the HFN (scale bar shows 10 µm). Fluorescence intensity profiles are plotted below the images showing a quantitative increase in fluorescence up to 100s after application of voltage bias (scale bar shows 3µm). Due to measurements being diffraction limited, the fluorescence appeared to be larger than the dimensions of the HFN despite being confined to the inside of the pore. The low-intensity fluorescence inside the nanopipette at t=0s which is attributed to the autofluorescent PVA-OH hydrogel confirms the presence of hydrogel within the first micron of the nanopipette tip (SI Figure S8). (c) Ionic current recordings of 250bp dsDNA translocations in the standard nanopipette (red) and the PVA-OH HFN (black) at three applied voltages (i) 400 mV, (ii) 500 mV, and (iii) 600 mV (SI Figure S9). Measurements were performed using a 5 kHz low-pass filter, and traces were resampled for visualization purposes (20 ms resampling rate). The SNR expressed as the ratio between average peak current and standard deviation of noise (10s trace, resampled at 12ms), was consistent across all three voltages at 12.3, 12.5 and 11.4 for 400 mV, 500 mV and 600 mV, respectively. (d) Voltage dependence of peak current (left column) and

dwell time (right column) for dsDNA translocations in the PVA-OH HFN, where average peak currents were 26±1 pA, 30±1 pA and 37±1 pA for 400 mV, 500 mV and 600 mV, respectively and average dwell time were 230±25 ms, 180±16 ms, and 170±12 ms for 400mV, 500mV, and 600mV, respectively.

The electrical and ion transport properties of nanopores can be investigated by examining current-voltage (IV) curves. These characteristic curves reflect essential nanopore properties, including charges and geometry, which may be tuned to achieve desirable effects including ion selectivity. IV curves were thus acquired for the PVA-OH HFN and a nanopipette filled with 100mM KCl solution (used here as a reference) (Figure 2a). The conductance, calculated from the linear region (+/- 100mV) of the IV curves, was G= 2.7±0.2 nS (N=5) for the HFN compared to G= 3.7±0.2 nS (N=6) for the standard solution-filled nanopipette. The reduced conductance in the hydrogel configuration was attributed to the higher resistance caused by the non-conductive neutral polymer fibers occupying the nanopore sensing region.

Unmodified quartz nanopores exhibited non-linear IV response and an ionic current rectification ratio of R = 2.3±0.3 (at ±400mV), which was consistent with observations for negatively charged glass nanopores, and is traditionally attributed to a combination of two effects: (i) asymmetrical geometry of the tip causing a difference in the limiting transport rates into and out of the nanopore, and (ii) surface charge leading to permselectivity to chloride ions.[55, 56] In the case of HFNs, the rectification ratio was higher, R = 2.8±0.6 (at ±400 mV), which considering the charge-free nature of the hydrogel, can most likely be attributed to a change in nanopore internal geometry owing to the nanoporous hydrogel mesh structure. Importantly, no significant difference in background noise level was observed between HFN and the bare nanopipettes (SI Figure S10).

For a detailed investigation of how the physical and chemical properties of our engineered hydrogels could affect DNA transport through solid-state nanopores, we used short dsDNA fragments ranging between 100 and 500bp, a size regime similar to that of cfNAs.

Remarkably, individual translocation events (current depletions) of 250bp DNA fragments were easily detectable in the HFN (Figure 2c) with a high signal-to-noise ratio (SNR), while for unmodified nanopipettes of the same diameter, individual translocation events could not be detected (SI Figure S11). Increasing the voltage across the HFN resulted in a minimal increase in peak current signals, but the dwell times were substantially slower than those reported in the literature using other solid-state nanopore configurations (Figure 2d).[9] For example, the average velocity for dsDNA through the HFN is 0.5 μm/s (500 mV bias, 22 nm pore), which is over 4 orders of magnitude slower than velocities reported in the literature for conventional (unmodified) solid-state nanopores: 1.0 cm/s (120 mV bias, 10 nm SiN pore, 1M KCl),[57] 0.8 cm/s (500 mV bias; 40 nm quartz nanopipette; 1M KCl),[52] and 1.1 cm/s (500mV bias, 7.5 nm quartz nanopipettes, 1M and 0.5M KCl).[53, 58]

This significant slowdown of translocation in HFNs was further characterized by single-molecule fluorescent imaging. To this end, 250bp dsDNA (800 pM) was fluorescently stained with a DNA intercalator (YOYO-1) and translocation events were monitored in real-time, for 2 min, with an emCCD camera (25 ms exposure time, λexc = 488 nm). Upon the application of voltage, unlike in the standard configuration **(**SI Figure S11), an accumulation of fluorescently labeled DNA could be observed at the tip of the nanopipette, and that spreads up to 5μm within the pipette (Figure 2b).

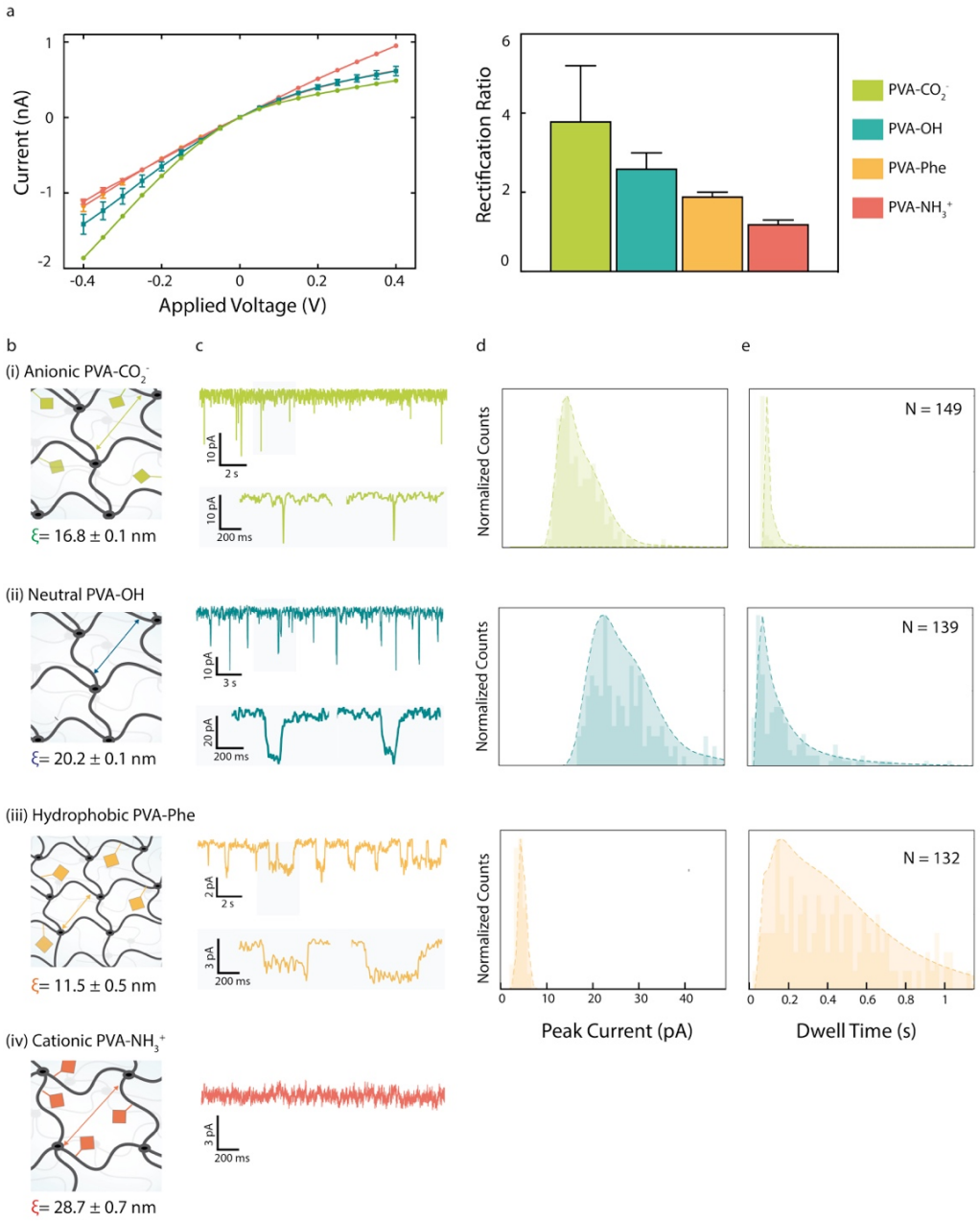

Figure 3. Detection of 250bp dsDNA translocations in four chemically distinct HFNs**.** (i) PVA-CO_2^-, (ii) PVA-OH, (iii) PVA-Phe and (iv) PVA-NH_3^+. (a) I-V curves (left) of the four HFNs showing deceasing rectification ratio (right) with decreasing negative charge. (b) Schematic representation of the hydrogel mesh structure within the HFN, where diamond structures represent chemical moieties; calculated mesh sizes (ε) are also reported. (c) Current-time traces of 250bp dsDNA translocations (600 pM) conducted in the various HFNs (500 mV bias). For visualization purposes, all traces were resampled at 20 ms except for PVA-CO_2^- trace (resampled at 5 ms). Dependence of peak current (d) and dwell time (e) on the chemical functionality within the HFN. No translocations were detectable in the PVA-NH_3^+ HFN; however, translocations of higher DNA fragment sizes such as 500bp dsDNA were detectable with high SNR (SI Figure S12).

In addition to slowing transport and analyte residence time in the nanopore, methods that can induce selectivity are critical for nanopore and biosensor detection in general and can enable discrimination of target analytes in complex media. Chemical modification of the hydrogel represents a simple and a tunable solution to nanopore surface modification for inducing sensing selectivity by controlling the surface charge and porosity. HFNs were engineered from three chemically-distinct macromers, prepared from the original PVA-OH by addition of (i) anionic carboxylate (PVA-CO_2^-), (ii) hydrophobic aromatic (PVA-Phe) and (iii) cationic ammonium (PVA-NH_3^+) moieties (Figure 3).

IV responses were measured for each HFN type, with all hydrogels prepared at the same macromer concentration of 15 wt% (Figure 3a). The effect on ion transport was investigated by calculating the rectification ratios of the four types of pipettes, at ±400 mV. As described earlier, the non-functionalized PVA-OH exhibited current rectification consistent with negatively-charged conical nanopores, with R=2.6±0.4. The PVA-CO_2^- HFN exhibited stronger negative rectification with R= 3.8±1.4, which was attributed to the enhanced negative surface charge resulting in a more substantial permselectivity to chloride anions. In contrast, the positively-charged PVA-NH_3^+ HFN exhibited almost no current rectification, with R=1.2±0.1. This decrease of current rectification can be explained by the positive charges on the hydrogel neutralizing the negative pore walls. Similarly, the PVA-Phe HFN showed lower negative rectification compared to the bare PVA-OH, with R=1.9±0.1. This may be due to the introduced hydrophobic groups that minimize the effect of charged pore walls. As expected, modifying the chemical properties of the hydrogel not only modulated the ion transport properties of the nanopore, but it also affected the nanopipette's conductance (SI Table S13).

Chemical modifications to the hydrogel with as few as 1-7 functionalities per chain resulted in significant changes to the physical and electrical properties of the nanopipettes. We thus sought to investigate how these changes may affect DNA transport by conducting translocation experiments with 250bp dsDNA (Figure 3). For the hydrophobic 10 wt% PVA-Phe HFN, it

was possible to detect DNA translocation events with longer dwell times compared to the unmodified PVA-OH, owing at least partly to the smaller mesh size (Figure 3iii). While the mean current was much smaller than with PVA-OH, the SNR (7.9 ± 2.1) was sufficient to allow detection under our experimental conditions. In the case of the anionic PVA-CO_2^-, a 10 wt% gel was not investigated as it produced a weakly crosslinked network. However, 15 wt% PVA-CO_2^- allowed for the detection of 250bp DNA with sufficient SNR and measurable dwell times (Figure 3i). Compared to the cationic hydrogel, this hydrogel had a smaller mesh size but also available negative charges. In this case, an increased electroosmotic force will be acting against the electrophoretic force, slowing down DNA transport into the nanopipette. For both the 10 wt% and 15 wt% PVA-NH_3^+ nanopipettes, no translocations were detectable (Figure 3iv). This may be partly attributed to the much larger pore sizes in this cationic hydrogel minimizing DNA interactions with the polymer fibers. Furthermore, in this configuration, both the electrophoretic and electroosmotic forces act in the same direction to drive DNA into the nanopipette.

In addition to controlling nanopore chemistry, controlling nanopore size can significantly improve SNR. In our initial experiments with HFN (Figure 2c), the average mesh size of the PVA-OH hydrogel was comparable to the size of the nanopore (20 nm and 22 nm, respectively). Increasing the nanopipette diameter from 22 to 50 nm diameter and keeping the PVA-OH hydrogel the same (average mesh size of 20 nm), did not affect the single-molecule translocation statistics (e.g., similar dwell times) of the HFN (SI Figure S14). These results indicated that it is in fact the properties of the hydrogel that control analyte transport. Thus, the dwell time of analytes in HFN could be controlled and adjusted by simply tuning the hydrogel mesh size rather than the (fixed) glass nanopipette aperture size. To this end, we used two strategies: (i) increasing fiber concentration (i.e., varying polymer weight percent from 10 to 15%) and (ii) increasing methacrylation from 1.4 to 5 mol%. IV curves of the standard 10 wt% PVA-OH HFN (1.4 mol % methacrylation) were overlaid with that of the two physically

modified hydrogels with increased crosslink density (SI Figure S15). Reduction in mesh size, by either increasing fiber concentration or increasing methacrylation, resulted in slower translocation speeds. Varying methacrylation, however, appeared as the preferred strategy (Figure 4). Increasing fiber concentration led to a significant drop in SNR (SI Figure S16) most likely caused by a reduction in the volume of conductive solution within the denser polymer.

With the emergence of cfNAs as clinically relevant biomarkers and with cfNA size profiling becoming a promising alternative to sequencing-based techniques,[59, 60] we investigated whether HFN could detect fragments the size of endogenous cfNAs (c.a. 100bp) and could discriminate between fragments of different sizes. For this application, we engineered HFNs using the PVA hydrogel with the highest crosslink density (i.e., 5 mol% methacrylation). After translocating 250bp DNA, the same pipette was moved into a bath containing 100bp DNA at 600 pM (Figure 4a). In Figure 4b, a comparison of the peak current of translocations with 100bp and 250bp are presented at three different voltages showing a voltage-dependent and size-dependent trend. Under the same experimental conditions, 100bp DNA translocations were detectable with a very high SNR (Figure 4c).

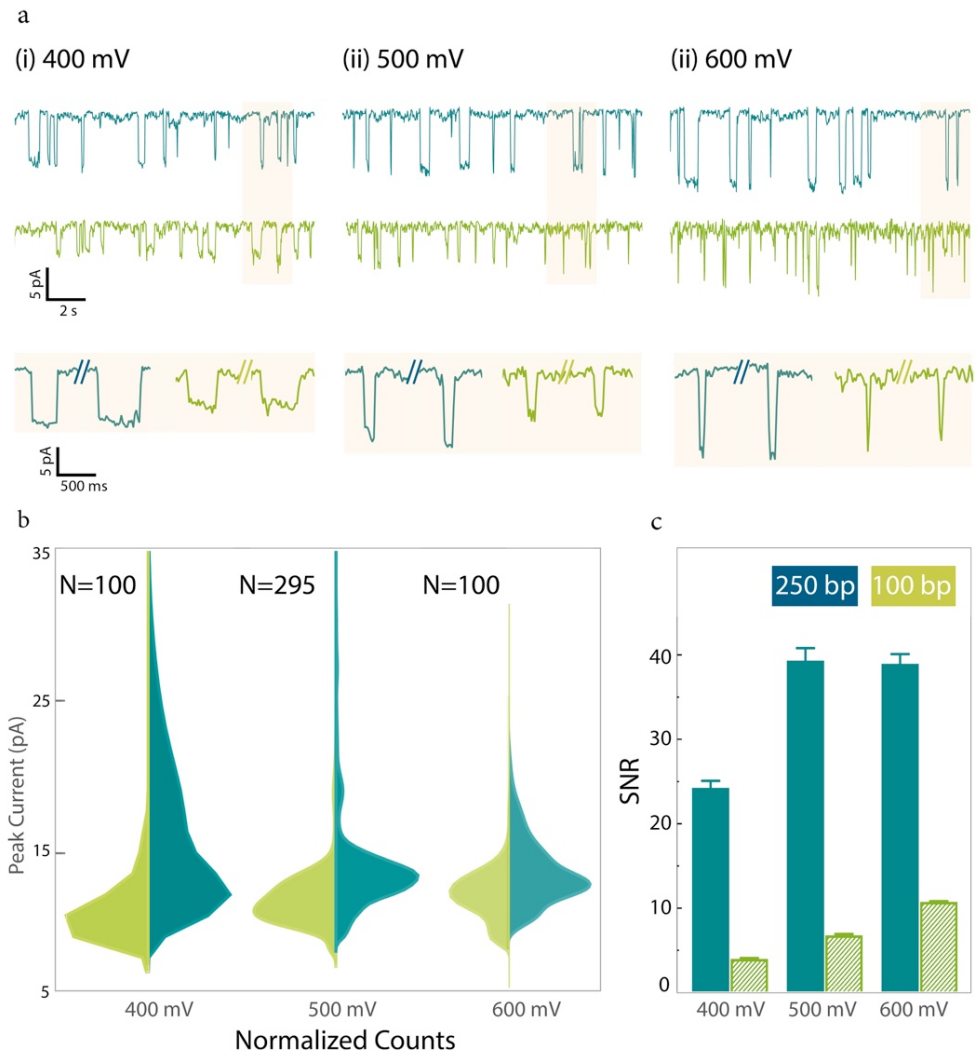

Figure 4. Detection and size profiling of small dsDNA fragments in HFNs. (a) Ionic current traces of 250bp DNA (blue, top) and 100bp dsDNA (green, bottom) at three applied voltages (resampled at 20 ms for visualization purposes;) (SI Figure S3). (b) Peak current dependence on applied voltage for 250bp dsDNA (blue, right) and 100bp dsDNA (green, left). (c) SNR, expressed as the ratio between the average peak current and the standard deviation of noise (3s trace, resampled at 5ms), was calculated for the 250bp dsDNA translocations (blue) and 100bp dsDNA translocations (green) at three applied voltages.

Based on our combined HFN data, it is apparent that the sensitivity and efficiency of analyte detection are enhanced when the average mesh size of the hydrogel is less than half the size of the analyte. Importantly, it was possible to detect both analytes which were longer and shorter than the persistence length of dsDNA (50 nm). In the case of 100bp dsDNA, fragments behave like rigid rods of 34 nm,[61] and were efficiently detected by the highly methacrylated PVA-OH with a mesh size of 12.0 ±0.2 nm. For detecting longer analytes, such as 250bp dsDNA, it was

possible to use hydrogels with a larger mesh size of 20.2±0.5 nm (Figure 3ii) which allowed for a higher degree of conformational flexibility within the hydrogel matrix.

The hydrogel within the nanopipette can be modelled as a network of crosslinked polymer fibres which give rise to a matrix of interconnected pores. As shown in Figure 5a, this can be represented as a layered architecture, each layer consisting of an array of pores whose diameters are defined by the physicochemical parameters of the engineered hydrogel. This irregular network acts as a barrier for the motion of molecules such as dsDNA. In fact, compared to the transport occurring in conventional conical-shaped glass nanopores, the time of flight of DNA molecules threading through HFNs is considerably larger. This is explained by the prolonged time required for the molecules to travel across the complex hydrogel matrix. In addition, the ionic current drop corresponding to the translocation of a single molecule in an HFN appeared to be characterized by discrete step-like drops (Figure 5c). One can assume that these stepwise changes are associated with the DNA movement from one pore to another, through the layers of the hydrogel. This model is consistent with our experimental data showing that molecular transport with the HFNs and ionic current blockades were strongly dependent on DNA size (Figure 5b). Longer DNA fragments have to thread across an increasing number of pores which in turn leads to larger current blockades with values ranging from 10pA for 100bp to 100pA for 1.5kbp DNA.

Based on our proposed mechanism, we anticipated that the transport of much larger DNA fragments (>kbp) would be significantly hindered and this process of molecular transport would become impossible. By using 10kbp dsDNA as a model, we were in fact able to observe this effect both optically (Figure 5d) and electrically (Figure 5e). Under positive voltage bias, single 10kbp DNA molecules became trapped at the HFN tip and were easily excluded by briefly reversing the potential.

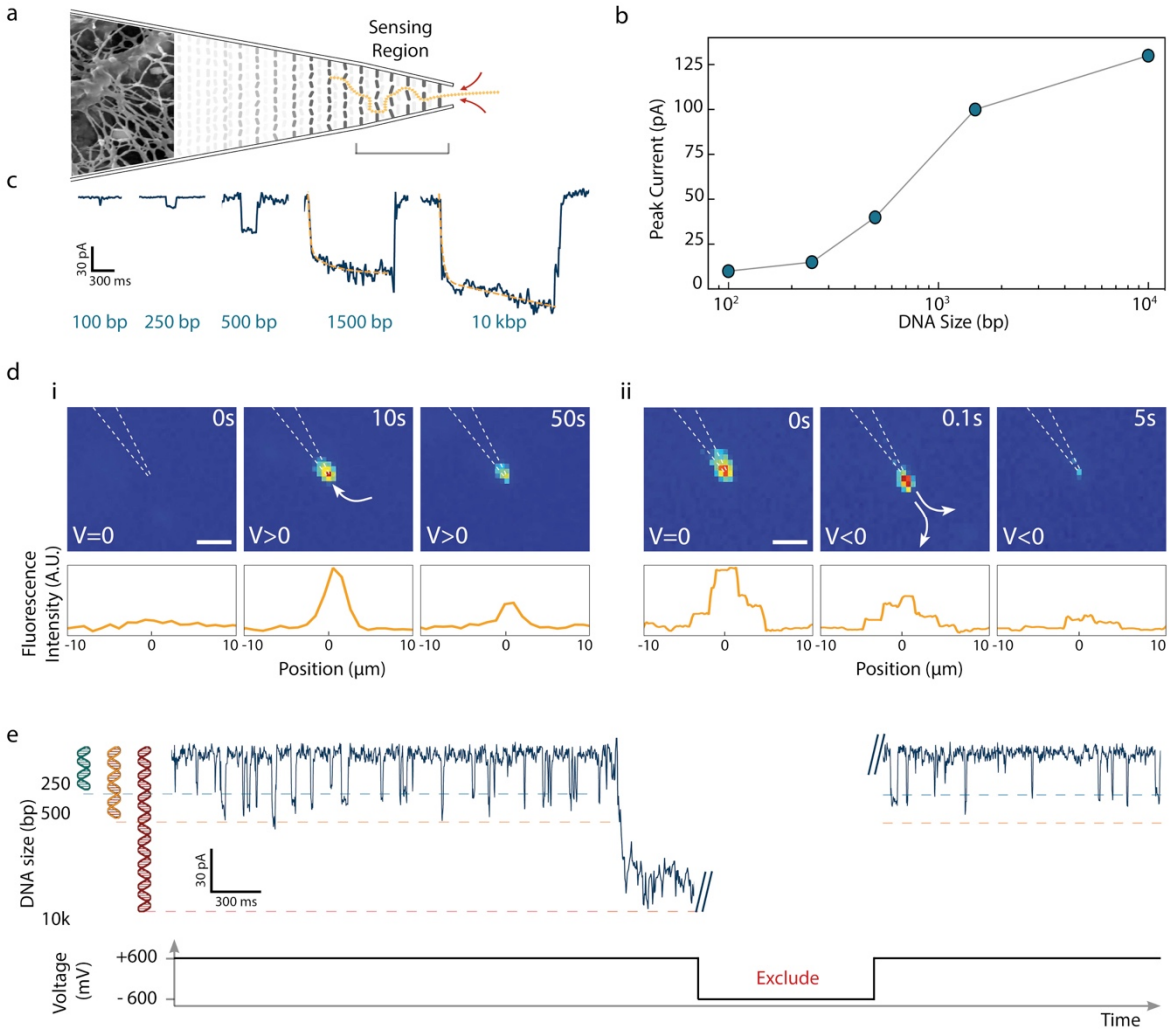

Figure 5. (a) Schematic representation of the proposed mechanism of dsDNA translocations through HFNs. The crosslinked polymer network of hydrogel within the nanopipette can be represented as a layered architecture with each layer consisting of an array of pores**.** As DNA travels through the complex network, it blocks pores giving rise to size-dependent current blockades and it is slowed down giving rise to long dwell times**.** (b) Plot of average peak current dependence on dsDNA size ranging from 100bp to 10kbp for the optimal high methacrylate PVA-OH HFN (600mV bias), showing a size-dependent trend. (c) Shape of representative ionic current depletions for a range of dsDNA sizes for the PVA-OH HFN (600mV bias). (d) Optical tracking of individual YOYO-1 labelled 10kbp dsDNA molecules which are significantly hindered at the HFN tip. Fluorescence images were recorded following the protocol outlined in Figure 2b. (i) Upon the application of a positive voltage bias after t=0s, a single DNA molecule is trapped at the HFN tip. The molecule remains at the tip for over 50s but fluorescence intensity decreases due to photobleaching within this timescale. (ii) Once a single 10kbp molecule is trapped at the tip at t=0s, the application of a negative voltage bias forces the DNA molecule out of the HFN, evident by the motion of the molecule at t=0.1s and disappearance of fluorescence at 5s. (scale bars show 2μm). (e) Current-time trace (600 mV bias) showing size-selective sampling of short DNA from a heterogenous DNA mixture containing short and long dsDNA strands. Based on the mechanism in (a), short DNA (<kbp) can travel through the pore network while longer DNA are significanlty hindered. If trapped at the HFN tip, 10kbp DNA can be ejected/excluded by briefly reversing the applied potential as demonstrated optically in (d.ii).

To exploit this mechanism and demonstrate suitability of HFNs in future clinical applications, a heterogenous mixture of DNA containing both short (250bp at 400pM and 500bp at 200pM) and long (10kbp at 100pM) DNA fragments was prepared, similar to conditions in complex biofluid samples. Interestingly for fcfNA sensing applications, our optimized high methacrylate PVA-OH HFN was capable to selectively sample the short dsDNA fragments (250bp and 500bp) while excluding the large 10kbp dsDNA from the multi-population mixture (Figure 5e). Unlike previously reported studies based on drilled nanopores and requiring custom high bandwidth amplifiers,[62, 63] detection of short dsDNA fragments and size exclusion was here achieved using simple large nanopipettes, low salt concentrations and a conventional amplifier.

In summary, we have developed a new generation of hybrid hydrogel-filled nanopore (HFN) sensors that can detect dsDNA fragments with single-molecule resolution and are suitable for the detection of short dsDNA fragments, under near-physiological conditions of salt and pH. We have demonstrated that using engineered hydrogels with mesh sizes smaller than the nanopore aperture offers greater control over the DNA translocation process by enabling fine-tuning of nanopore sensors in terms of porosity and perhaps more importantly charge. Importantly, we showed that it was possible to selectively detect dsDNA fragments ranging from 100bp to 500bp long, a size regime that overlaps well with that of endogenous cfNA biomarkers found in body fluids, while filtering out larger (>10kbp) fragments. DNA translocation through our HFNs is as slow as 1.4bp/ms and can be finely tuned by adjusting the chemical and physical properties on the inside hydrogel, a strategy that is significantly easier and more robust than currently available alternatives based on complex modifications of the nanopore aperture. HFNs could have valuable applications in the biomedical research field where detection of low copy numbers of analyte in complex biofluids are required, most notably cancer diagnostics (cfNA from tumor cells being typically shorter than that from somatic cells)

and prenatal testing (fetal cfNA in mother's blood being significantly shorter than that of the maternal origin). Working under near physiological conditions of salt and pH, HFNs are also perfectly suited for the detection of more sensitive analytes such as proteins and protein-DNA complexes.

MATERIALS AND METHODS

Macromer synthesis. To a stirred solution of PVA in anhydrous dimethylsulfoxide (DMSO) at 20 wt% was slowly added, at 60°C and under nitrogen, a stoichiometric amount of 2-Isocyanatoethyl methacrylate (2-ICEMA, Sigma). The reaction mixture was then stirred (at 60°C and under nitrogen) for an additional 4h. Acetalization of the methacrylated PVA was then performed at 40°C in anhydrous DMSO by dropwise addition of a solution of the corresponding acetal (4-aminobutyraldehyde diethyl acetal (Sigma) for PVA-NH_3^+; 3,3-dimethoxypropanoic acid (Fluorochem) for PVA-CO_2^-, Phenylacetaldehyde dimethyl acetal (Sigma) for PVA-Phe) in anhydrous DMSO. A solution of concentrated HCl (37N) was then added dropwise to bring the pH to below 1. After 30 min, the reaction was quenched by rapidly increasing the pH to 8 via the addition of concentrated ammonia. The polymer was finally dialyzed (MWCO 12 kDa) against water for three days then lyophilized to obtain the desired macromer as a white product.

Hydrogel engineering. To convert the synthesized polymers into hydrogels, a desired weight percentage of the polymer was prepared in 100m M KCl, 10mM Tris-EDTA buffer (pH 8.0) solution, to which the photoinitiator Irgacure 2959 (Sigma) was added at a final concentration of 0.1 wt%. The solution was then irradiated with UV light in a BLX-315 UV crosslinker (315 nm, 3min, 1J energy).

Analysis of hydrogels' network structure and physical properties. Nine hydrogel disks were prepared then weighed to provide the initial dry mass, m_0. Three disks were frozen and lyophilized to provide the dry weights (md), while the rest were swelled in water at room temperature. After 1 day and 7 days, the disks were weighted to provide the swollen masses (ms_1 and ms_7 respectively), then lyophilized to provide the dry masses after swelling (md). From the masses recorded, the following characteristic parameters were calculated: actual macromer fraction, mass swelling ratio, % sol fraction (fraction of macromers that have not been incorporated into the crosslinked network), and the volumetric swelling ratio (Q) (amount of water contained inside the hydrogels).

Hydrogel-Filled Nanopipettes (HFN) engineering. Quartz nanopipettes were fabricated using laser-assisted pipette pulling of single-barreled quartz capillaries (I.D., 0.5 mm; O.D., 1 mm; length, 7.5 cm; World Precision Instruments) using a laser pipette puller (P-2000, Sutter Instruments).[24] The pulling produced a sharp tip terminating with a pore of 22 nm diameter.[25] Pipettes were then filled with a solution of PVA methacrylate prepared in 100 mM KCl, 10 mM Tris-EDTA (pH 8.0) solution containing 0.1 wt% of Irgacure 2959, and gelation was performed in a BLX-315 UV crosslinker (1J Energy, 315 nm, Consort). An Ag/AgCl electrode (patch/working electrode) was then inserted inside the pipette. A detailed description of the fabrication process for an HFN can be found in SI Note S17.

DsDNA translocation through HFNs. HFNs were immersed into a 100 mM KCl, 10 mM Tris-EDTA (pH 8.0) solution bath containing an Ag/AgCl ground electrode. Electrolyte ionic strength and pH chosen for nanopore sensing were near-physiological. Unless indicated otherwise, DNA translocation experiments were performed by applying a positive potential at the patch electrode, thus inducing the translocation of dsDNA from the outside to the inside of the nanopipette (i.e., from solution to hydrogel). Current vs. time traces were acquired at a 100

kHz sampling rate with a 5 kHz low-pass Bessel filter. Representative translocation data consisted of at least 130 events recorded per pipette, for at least three different pipettes under the same experimental conditions. Data can be recorded for extended periods of time without issues, where at least 10-15 min are recorded per voltage per pipette, as demonstrated in SI Figure S18.

Acknowledgement

DAS acknowledges the support by an Imperial College Ph.D. scholarship. JBE has been funded in part by an ERC starting (NanoP), proof of concept (NanoPP), and consolidator (NanoPD) grants. AI and JBE acknowledge support from EPSRC grant EP/P011985/1. Al acknowledges the support of the IC Research Fellowship.

Supporting Information

The accompanying supporting information detail the following; chemical synthesis, NMR analysis of engineered hydrogels, SEM images of the engineered hydrogels and the nanopores, swelling study and mesh size analysis, and additional experimental data on DNA translocation in engineered hydrogels. This material is available free of charge via the Internet at http://pubs.acs.org

References

1. Justin, G. J.; Katharina, G. *Angewandte Chemie International Edition* **2016,** 55, (38), 11354-11366.
2. Underhill, H. R.; Kitzman, J. O.; Hellwig, S.; Welker, N. C.; Daza, R.; Baker, D. N.; Gligorich, K. M.; Rostomily, R. C.; Bronner, M. P.; Shendure, J. *PLOS Genetics* **2016,** 12, (7), e1006162.
3. Mouliere, F.; Rosenfeld, N. *Proceedings of the National Academy of Sciences of the United States of America* **2015,** 112, (11), 3178-3179.
4. Jahr, S.; Hentze, H.; Englisch, S.; Hardt, D.; Fackelmayer, F. O.; Hesch, R.-D.; Knippers, R. *Cancer Research* **2001,** 61, (4), 1659-1665.

5. Ellinger, J.; Müller, S. C.; Stadler, T. C.; Jung, A.; von Ruecker, A.; Bastian, P. J. In *The role of cell-free circulating DNA in the diagnosis and prognosis of prostate cancer*, Urologic Oncology: Seminars and Original Investigations, 2011; Elsevier: pp 124-129.
6. Gormally, E.; Caboux, E.; Vineis, P.; Hainaut, P. *Mutation Research/Reviews in Mutation Research* **2007,** 635, (2), 105-117.
7. Jung, K.; Fleischhacker, M.; Rabien, A. *Clinica Chimica Acta* **2010,** 411, (21), 1611-1624.
8. Miles, B. N.; Ivanov, A. P.; Wilson, K. A.; Dogan, F.; Japrung, D.; Edel, J. B. *Chemical Society Reviews* **2013,** 42, (1), 15-28.
9. Venkatesan, B. M.; Bashir, R. *Nature Nanotechnology* **2011,** 6, 615.
10. M., M. M.; Jijin, Y.; R., H. A. *Scanning* **2012,** 34, (2), 101-106.
11. Murali, V. B.; Brian, D.; Sukru, Y.; Nicholas, W.; Ivan, P.; Rashid, B. *Advanced Materials* **2009,** 21, (27), 2771-2776.
12. Wanunu, M.; Dadosh, T.; Ray, V.; Jin, J.; McReynolds, L.; Drndić, M. *Nature Nanotechnology* **2010,** 5, 807.
13. Wanunu, M.; Meller, A. *Nano Letters* **2007,** 7, (6), 1580-1585.
14. Michiel van den, H.; Adam, R. H.; Meng Yue, W.; Henny, W. Z.; Cees, D.; Nynke, H. D. *Nanotechnology* **2010,** 21, (11), 115304.
15. Eric, B.; Harold, K.; Vincent, T.-C.; Michel, G. *Nanotechnology* **2012,** 23, (40), 405301.
16. Kim, Y.-R.; Min, J.; Lee, I.-H.; Kim, S.; Kim, A.-G.; Kim, K.; Namkoong, K.; Ko, C. *Biosensors and Bioelectronics* **2007,** 22, (12), 2926-2931.
17. Yameen, B.; Ali, M.; Neumann, R.; Ensinger, W.; Knoll, W.; Azzaroni, O. *Small* **2009,** 5, (11), 1287-1291.
18. Ren, R.; Zhang, Y.; Nadappuram, B. P.; Akpinar, B.; Klenerman, D.; Ivanov, A. P.; Edel, J. B.; Korchev, Y. *Nature Communications* **2017,** 8, (1), 586.
19. Wang, L.; Zhang, H.; Yang, Z.; Zhou, J.; Wen, L.; Li, L.; Jiang, L. *Physical Chemistry Chemical Physics* **2015,** 17, (9), 6367-6373.
20. Iqbal, S. M.; Akin, D.; Bashir, R. *Nature Nanotechnology* **2007,** 2, 243.
21. Wei, R.; Gatterdam, V.; Wieneke, R.; Tampé, R.; Rant, U. *Nature Nanotechnology* **2012,** 7, 257.
22. Ali, M.; Yameen, B.; Neumann, R.; Ensinger, W.; Knoll, W.; Azzaroni, O. *Journal of the American Chemical Society* **2008,** 130, (48), 16351-16357.
23. Yusko, E. C.; Johnson, J. M.; Majd, S.; Prangkio, P.; Rollings, R. C.; Li, J.; Yang, J.; Mayer, M. *Nature Nanotechnology* **2011,** 6, 253.
24. Lepoitevin, M.; Ma, T.; Bechelany, M.; Janot, J.-M.; Balme, S. *Advances in Colloid and Interface Science* **2017,** 250, 195-213.
25. Brazel, C. S.; Peppas, N. A. *Biomaterials* **1999,** 20, (8), 721-732.
26. Peppas, N. A.; Keys, K. B.; Torres-Lugo, M.; Lowman, A. M. *Journal of controlled release* **1999,** 62, (1), 81-87.
27. Bryant, S. J.; Anseth, K. S. *Biomaterials* **2001,** 22, (6), 619-626.
28. Kobayashi, M.; Toguchida, J.; Oka, M. *Journal of Biomedical Materials Research Part A* **2001,** 58, (4), 344-351.
29. Young, C.-D.; Wu, J.-R.; Tsou, T.-L. *Biomaterials* **1998,** 19, (19), 1745-1752.
30. Sirkar, K.; Pishko, M. V. *Analytical Chemistry* **1998,** 70, (14), 2888-2894.
31. Zeng, X.; Liu, J.; Zhang, Z.; Kong, S. *Int. J. Electrochem. Sci* **2015,** 10, 8344-8352.
32. Kiyonaka, S.; Sada, K.; Yoshimura, I.; Shinkai, S.; Kato, N.; Hamachi, I. *Nature Materials* **2003,** 3, 58.
33. Yan, L.; Zhu, Z.; Zou, Y.; Huang, Y.; Liu, D.; Jia, S.; Xu, D.; Wu, M.; Zhou, Y.; Zhou, S.; Yang, C. J. *Journal of the American Chemical Society* **2013,** 135, (10), 3748-3751.
34. Uhlich, T.; Ulbricht, M.; Tomaschewski, G. *Enzyme and Microbial Technology* **1996,** 19, (2), 124-131.

35. Al Sulaiman, D.; Chang, J. Y. H.; Ladame, S. *Angewandte Chemie (International Ed. in English)* **2017,** 56, (19), 5247-5251.
36. Kang, X.-f.; Cheley, S.; Rice-Ficht, A. C.; Bayley, H. *Journal of the American Chemical Society* **2007,** 129, (15), 4701-4705.
37. Culver, H. R.; Clegg, J. R.; Peppas, N. A. *Accounts of Chemical Research* **2017,** 50, (2), 170-178.
38. Tavakoli, J.; Tang, Y. *Polymers* **2017,** 9, (8), 364.
39. Jung, I. Y.; Kim, J. S.; Choi, B. R.; Lee, K.; Lee, H. *Advanced Healthcare Materials* **2017,** 6, (12).
40. Oka, M.; Noguchi, T.; Kumar, P.; Ikeuchi, K.; Yamamuro, T.; Hyon, S. H.; Ikada, Y. *Clinical Materials* **1990,** 6, (4), 361-381.
41. Noguchi, T.; Yamamuro, T.; Oka, M.; Kumar, P.; Kotoura, Y.; Hyonyt, S. H.; Ikadat, Y. *Journal of Applied Biomaterials* **1991,** 2, (2), 101-107.
42. Paradossi, G.; Cavalieri, F.; Chiessi, E.; Spagnoli, C.; Cowman, M. K. *Journal of Materials Science: Materials in Medicine* **2003,** 14, (8), 687-691.
43. Squires, A. H.; Hersey, J. S.; Grinstaff, M. W.; Meller, A. *Journal of the American Chemical Society* **2013,** 135, (44), 16304-16307.
44. Tang, Z.; Liang, Z.; Lu, B.; Li, J.; Hu, R.; Zhao, Q.; Yu, D. *Nanoscale* **2015,** 7, (31), 13207-13214.
45. Waugh, M.; Carlsen, A.; Sean, D.; Slater, G. W.; Briggs, K.; Kwok, H.; Tabard-Cossa, V. *Electrophoresis* **2015,** 36, (15), 1759-1767.
46. Schmedlen, R. H.; Masters, K. S.; West, J. L. *Biomaterials* **2002,** 23, (22), 4325-4332.
47. Sanjust, E.; Cocco, D.; Curreli, N.; Rescigno, A.; Sollai, F.; Bannister, J. V. *Journal of Applied Polymer Science* **2002,** 85, (11), 2471-2477.
48. Carr, D. A.; Peppas, N. A. *Macromolecular Bioscience* **2009,** 9, (5), 497-505.
49. Peppas, N. A.; Merrill, E. W. *Journal of Polymer Science: Polymer Chemistry Edition* **1976,** 14, (2), 459-464.
50. Peppas, N. A.; Merrill, E. W. *Journal of Applied Polymer Science* **1977,** 21, (7), 1763-1770.
51. Bryant, S. J.; Davis-Arehart, K. A.; Luo, N.; Shoemaker, R. K.; Arthur, J. A.; Anseth, K. S. *Macromolecules* **2004,** 37, (18), 6726-6733.
52. Gong, X.; Patil, A. V.; Ivanov, A. P.; Kong, Q.; Gibb, T.; Dogan, F.; deMello, A. J.; Edel, J. B. *Analytical Chemistry* **2014,** 86, (1), 835-841.
53. Sze, J. Y. Y.; Kumar, S.; Ivanov, A. P.; Oh, S.-H.; Edel, J. B. *Analyst* **2015,** 140, (14), 4828-4834.
54. Ivanov, A. P.; Actis, P.; Jönsson, P.; Klenerman, D.; Korchev, Y.; Edel, J. B. *ACS Nano* **2015,** 9, (4), 3587-3595.
55. Wei, C.; Bard, A. J.; Feldberg, S. W. *Analytical Chemistry* **1997,** 69, (22), 4627-4633.
56. White, H. S.; Bund, A. *Langmuir* **2008,** 24, (5), 2212-2218.
57. Li, J.; Gershow, M.; Stein, D.; Brandin, E.; Golovchenko, J. A. *Nature Materials* **2003,** 2, 611.
58. Steinbock, L. J.; Otto, O.; Chimerel, C.; Gornall, J.; Keyser, U. F. *Nano Letters* **2010,** 10, (7), 2493-2497.
59. Jiang, P.; Lo, Y. M. D. *Trends in Genetics* **2016,** 32, (6), 360-371.
60. Yu, S. C. Y.; Chan, K. C. A.; Zheng, Y. W. L.; Jiang, P.; Liao, G. J. W.; Sun, H.; Akolekar, R.; Leung, T. Y.; Go, A. T. J. I.; van Vugt, J. M. G.; Minekawa, R.; Oudejans, C. B. M.; Nicolaides, K. H.; Chiu, R. W. K.; Lo, Y. M. D. *Proceedings of the National Academy of Sciences* **2014,** 111, (23), 8583-8588.
61. Allison, S.; Chen, C.; Stigter, D. *Biophysical Journal* **2001,** 81, (5), 2558-2568.
62. Carson, S.; Wilson, J.; Aksimentiev, A.; Wanunu, M. *Biophysical Journal* **2014,** 107, (10), 2381-2393.

63. Fraccari, R. L.; Carminati, M.; Piantanida, G.; Leontidou, T.; Ferrari, G.; Albrecht, T. *Faraday Discussions* **2016,** 193, (0), 459-470.